Dynamic Modeling, Stability Analysis and Power Management of Shipboard DC Hybrid Power Systems

Daeseong Park, *Student Member, IEEE*, and Mehdi Zadeh, *Member, IEEE*

***Abstract*—This paper proposes a framework for the stability analysis and control testing of marine hybrid power systems with DC power architecture. The dynamics of such active systems are increasingly influenced by interactive modes such as the highly dynamic loads and varying load sharing scenarios, electro-mechanical modes, and integration of energy storage systems (ESS). Hence, a dynamic model of the entire system is developed including the power electronics and ESS, electro-mechanical systems, different controllers–low level and high level– and propulsion loads. The proposed analytical model is used to establish not only the small-signal stability analysis but also time-domain simulations. Then, a set of dynamic analyses and tests has been performed to identify the stability challenges that a vessel may be exposed to during a real operation. The suggestions for improving the system performance are given as the control modification at different levels. To emulate the real operation, a ship operational profile is used for the tests. Finally, the proposed dynamic model is verified with the experimental results conducted in a full-scale hybrid power systems laboratory. The results show that the system dynamics can be affected significantly by the interaction of the high-level and low-level control of the converters, which is usually neglected in conventional models.**

***Index Terms*—Onboard DC power systems, hybrid electric ships, marine power systems, dynamic modeling, stability, energy storage systems.**

I. Introduction

Ship power systems (SPS) are developed with AC and DC architecture, using an AC main bus, namely AC switchboard, and a DC main bus/switchboard, respectively. The AC SPS (as shown in Fig. 1(a)) is an upgraded version as the well-known diesel-electric propulsion where the mechanical propulsion is replaced by the combination of diesel generator sets (gensets) and electric motors towards higher efficiency and flexibility. The energy efficiency can be further improved if the prime movers, i.e., engines, can work at lower speed ranges or further variable speed [1], leading to the development of DC SPS as a frequency-free propulsion system. These flexible and active power systems are standing on the capabilities of the power electronics [2] as shown in Fig. 1(b). DC SPS can also remove and/or reduce bulky transformers, frequency converters, and AC synchronization issues. Besides, the DC SPS topology becomes much more friendly to install energy storage systems

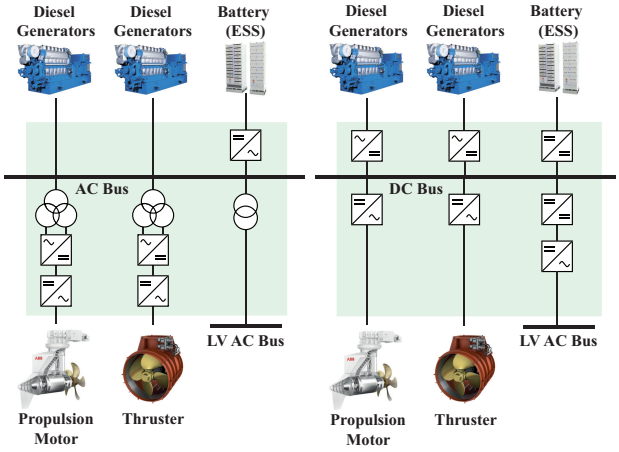

(a) AC SPS (b) DC SPS

Fig. 1: Simplified topology of marine power system (AC SPS vs DC SPS)

(ESS) [3] aiming at reduced fuel consumption and better voltage stability [4], [5]. However, despite the installation of ESS, large ships still require to have gensets because of the limited energy density of ESS (both weight and volume perspective). In DC SPS, different types of rectifiers are used such as diode front end (DFE), thyristor front end (TFE), and active front end rectifier (AFE) rectifier. The DC grid formed by DFE is a simple and economical solution because it does not require any switching devices and additional controllers. However, in this case, the DC voltage is only dependent on the AC voltage control [6] while TFE has the flexibility to step down the voltage, yet TFE cannot boost the voltage. AFE can control the DC voltage actively with higher control bandwidths and significantly better dynamic response [7]. However, the AFE-based solutions for high-power applications are expensive and require a proper stability analysis including the associated controllers.

The efficiency and flexibility of such hybrid power systems are highly dependent on high-level controllers, so-called power management system (PMS) and energy management system (EMS), which are responsible for the load sharing between the multiple power sources and storage systems. It should be noted that the gensets can be designed with various ratings (e.g. two larger gensets and two smaller gensets) due to technical reasons including the efficiency improvement at low-load operation and cost reduction. In the commercial AC

Manuscript received April 1, 2021; revised June 22, 2021; accepted September 23, 2021.

D. Park and M. K. Zadeh are with the Department of Marine Technology, Norwegian University of Science and Technology, Trondheim, 7056 Norway (e-mail: daeseong.park@ntnu.no; mehdi.zadeh@ntnu.no).

SPSs, the load-sharing between gensets is usually achieved by droop (frequency droop) and isochronous (zero droop gain) control as a widely adopted decentralized method because of its simplicity and the fact that it does not require any additional sensors and communications between the gensets. In this case, active and reactive power control are implemented using the engines' governors (GOV) and generators' automatic voltage regulators (AVR) [8]. The frequency droop is usually designed with equal load sharing between the gensets to avoid stability issues, except specific transient conditions (often ship maneuvering) where the increased load may be shared unequally [9]. However, equal load sharing is extensively applied in a very conservative way, so this practice does not offer the best efficiency of the system operation. In [10], it is shown that unequal load sharing between the gensets (and battery) provides better efficiency. Hence, the droop parameters, such as the droop gain and no-load frequency, must be chosen carefully.

In DC SPSs, the load-sharing is also achieved by DC voltage droop (inverse droop control) and isochronous control producing the voltage set-points for the low-level controllers. In the low-level control, the DC voltage control can be implemented depending on the power system topology, using either AVR, AVR and firing angle of TFE, or AFE rectifier. Therefore, the load sharing scheme should be adjusted depending on the rectifier type. Here, the AFE rectifier can provide very higher control flexibility compared to the AVR. The voltage set-point to the AFE controller is then produced by the droop, such that dynamic load changes are handled by changing the droop gain, i.e. higher droop gain enables to follow the load faster, however, by allowing relatively higher voltage deviations from the reference voltage [9]. Furthermore, the isochronous control can be assigned to one machine exclusively to handle transient loads faster than the droop-controlled machines.

The droop control is addressed widely in the literature. [11] proposes a nonlinear droop curve to secure the bus voltage regulation in the low load range and to have better current sharing accuracy in the heavy load range. [12] proposes V-I based droop control for diesel generators for the conventional AC power system and a hierarchical controller for the bidirectional DC-DC converters that interface energy storages installed inside the propulsion drive. In [12], a power control loop is added in the DC-DC converter control in order to compensate for the DG power fluctuations. In spite of the simple implementation, the droop control may be also challenging since the droop parameters and the reference voltage should be continuously updated with new power references. Besides, updating the droop gain with a big jump may also lead to sudden voltage drop/rise with consequent load increase/decrease respectively.

The previous research is missing to address the influence of dynamic load sharing on voltage stability. Those proposed load sharing schemes produce highly dynamic (unequal) load set-points, resulting in high voltage fluctuations with sudden jumps which compromise the stability as well as the load sharing accuracy. On the contrary, isochronous control is developed where the constant voltage reference is assigned at lower voltage levels. In this case, to reach the enhanced unequal load sharing, it is recommended to have a mid-level controller (e.g. PI controller) that adjusts voltage references to regulate the output powers from each power source [13], [14]. Then, AFEs and DC-DC converters should follow the dynamic references affecting the system stability and power quality. Therefore, it is required to analyze the interactions between multiple power sources and loads considering the dynamics of each sub-system and lower-level controller. The droop can also be replaced by a PI which needs to be tuned considering the system stability.

State-of-the-art research on the control design and stability analysis of DC SPS investigated the influence of design parameters on the system stability [15], and in particular finding the required capacitance and the cable length of the DC-grid as presented in [16]. Voltage stability is also studied against the negative effect of constant power loads (CPL) in [17]–[19]. Influence of controller parameters is also studied in the literature such as the effect of frequency and voltage droop gains on the AC power system stability [20], estimation of the stable voltage operation range for permanent magnet generator and diode rectifier [6], coordinated control of a hybrid-electric SPS [14], [21], three-layer control design of DC SPS [13] and study of a predictive control approach to regulating the DC voltage in hybrid-electric SPS [22].

Dynamic stability of DC microgrids has also been addressed in the literature such as large-signal and small-signal methods. In [23] a large-signal stability analysis is proposed for droop-controlled DC microgrids. However, based on this method, the system model shall be simplified otherwise it is not extendable to real applications. To overcome this issue, the well-known small-signal approach has been tested particularly for larger system models and real applications; in [18] eigenvalue analysis is used to evaluate the dynamic stability of the system under load conditions. The influence of CPL on dynamic stability is also investigated based on eigenvalues [24]–[26] and the system stability is improved thanks to modified load sharing and power set-points [27], [28]. Discrete-time approaches are also tested on DC power systems mainly for vehicular and aviation applications [29]. These models are accurate and reliable, yet not easy to be used in real-time applications.

Yet, the capabilities of the DC SPS are numerous and have brought many unexplored challenges. In such active systems, the system dynamics is shaped instantaneously by the interaction of the control system and the physical system. Marine propulsion has usually a highly dynamic and case-dependent load profile, and the dynamic load in line with the efficiency requirements and emission constraints demands a varying load sharing control which is normally developed and optimized inside EMS/PMS. The outcome of the EMS as instantaneous – and maybe optimal – power and voltage set-points will be given to the power units and will result in interactive dynamics. On the other hand, the large marine ESS are integrated into the hybrid SPS with fast power electronics with the original objective of improving the fuel efficiency, although it has specific influences on the system stability depending on the size and C-rate of the batteries. The high power AFE rectifiers are also becoming more accepted in the maritime industry thanks to the reduced price. It shapes the

system dynamics in a large extent by shifting the load sharing control from AVR to the AFE.

Even though the effect of the recent developments may be positive, they are to be investigated by expanding the dynamic models. Moreover, the mechanical part of the power system, such as engines, and the associated interactive modes are usually neglected or simplified in the conventional dynamic models of power systems. In other words, the state-of-the-art focused on the modeling of power converters, not considering the full-set of power systems including diesel engines and synchronous generators. The lack of the full-set of the dynamic model makes it difficult to analyze interactions between low-level and high-level control systems in the real and extreme ship operation conditions since the engine-generator systems still have a significant dynamic effect. In addition, the modeling work of the advanced power electronics (AFE rectifiers) to the AC subsystems in the shipboard hybrid power system has not been properly addressed in the previous studies. In the new paradigm of system operation, the power system is suffering from the varying profile on both electrical and mechanical parts (engine-generators), necessitating further expansion of the system model and inclusion of so-called electro-mechanical modes.

This paper is proposing a dynamic and stability framework to identify and investigate the stability issues related to the operation of onboard hybrid DC power systems. A set of dynamic tests has been performed– in both linearized small-signal domain and nonlinear time-domain– to cover the main control scenarios such as the load sharing between the power units. Here, the dynamic model of the system is extended to include the electro-mechanical system and its associated dynamic modes, which helps to study the engine-generators with both fixed and variable speed operation. A state-space model of the entire system (including the subsystems and controllers) is then developed and linearized to derive the system eigenvalues. Here, the focus of the modeling and analysis is to investigate the interactions of the low-level controller with the PMS under different control scenarios, in particular, unequal load sharing. Therefore, the switching effect of the converters is neglected and the converters are modeled based on averaging. In this case, the system dynamics are formed mainly by linear dynamics, and hence, the eigenvalues can be used safely for the stability analysis.

To ensure the stability of the DC SPS, some modifications have been suggested to the control system where the power and voltage set-points are produced and given to the AFE rectifiers and the DC-DC converter. The suggested controller applies only simple modifications to the conventional set-up by replacing the voltage droop with a constant set-point which is updated dynamically. In the load sharing, the control performance is further improved by modifying the droop and introducing integral terms. The performance of the presented PMS is also compared with the conventional load sharing methods.

The proposed dynamic model is used to test and validate different operating modes of the DC hybrid power system with various functioning of ESS, and various ship load profiles. It can be adopted easily in real ship operations to develop optimal and intelligent EMS. To emulate the ship operation, a real ship profile is used for the tests. Finally, the analytical model is validated with the experimental results from a full-scale laboratory with engine-generators, ESS, and propulsion loads. The results show the consistency of the proposed model and the experimental results in different operating modes with and without battery. Not only the electrical properties, but also the engine dynamics are compared in simulation and experiments.

The rest of this paper is organized as follows. In Section II, the case study of DC SPS is presented with the proposed modeling approach including the sub-systems and the load-sharing strategy. Section III gives stability analysis for the controller tuning and performance comparison with the time-domain simulation results. In Section IV, simulation results with a real ship operation profile and different types of battery operation and experimental results are presented to validate the effectiveness of the model under the unequal load sharing. In the end, Section V concludes this paper with the main findings of this work.

II. Modeling of the DC Hybrid Power System with Multi-layer Control System

In this section, the mathematical model of the DC hybrid power system is developed with its sub-systems and different control layers such as low-level control and PMS. The electric circuit diagram of the studied DC SPS is shown in Fig. 2, where the source sub-system is comprised of two diesel engine-generator sets and a battery system. The load sub-system is modeled as a CPL which represents the power regulated propulsion motor drives. The DC switchboard (distribution system) consists of 2 AFE rectifiers connecting gensets to the DC bus, a half-bridge DC-DC converter connecting the batteries to the DC grid, and a capacitor bank (C_{dc}).

A. AC Subsystem: Diesel Engine Generators with GOV and AVR

- Engine part with fuel injection control (z_i):

For the diesel engine, as the generator's prime mover, a first order model is used [30]. Therefore, the engine model can be represented as:

$$\dot{T}_{m,i} = \frac{1}{T_{de,i}}(-T_{m,i} + z_i) \tag{1}$$

$$\dot{X}_{gov,i} = \omega_i^* - \omega_i \tag{2}$$

$$z_i = k_{p,gov_i}(\omega_i^* - \omega_i) + k_{i,gov_i} X_{gov,i} \tag{3}$$

where $T_{m,i}$ [pu] represents a mechanical torque, z [pu] is fuel index and $T_{de,i}$ [s] is time constant of the diesel engine. The fuel index is determined by a PI controller that includes the dynamics of GOV and fuel supply system with PI-gains (k_{p,gov_i} and k_{i,gov_i}) in order to regulate the engine shaft speed (ω_i [pu]) to its reference (ω_i^*) expressed with an error dynamics ($X_{gov,i}$). The subscript i represents the i^{th} number of the equipment hereafter.

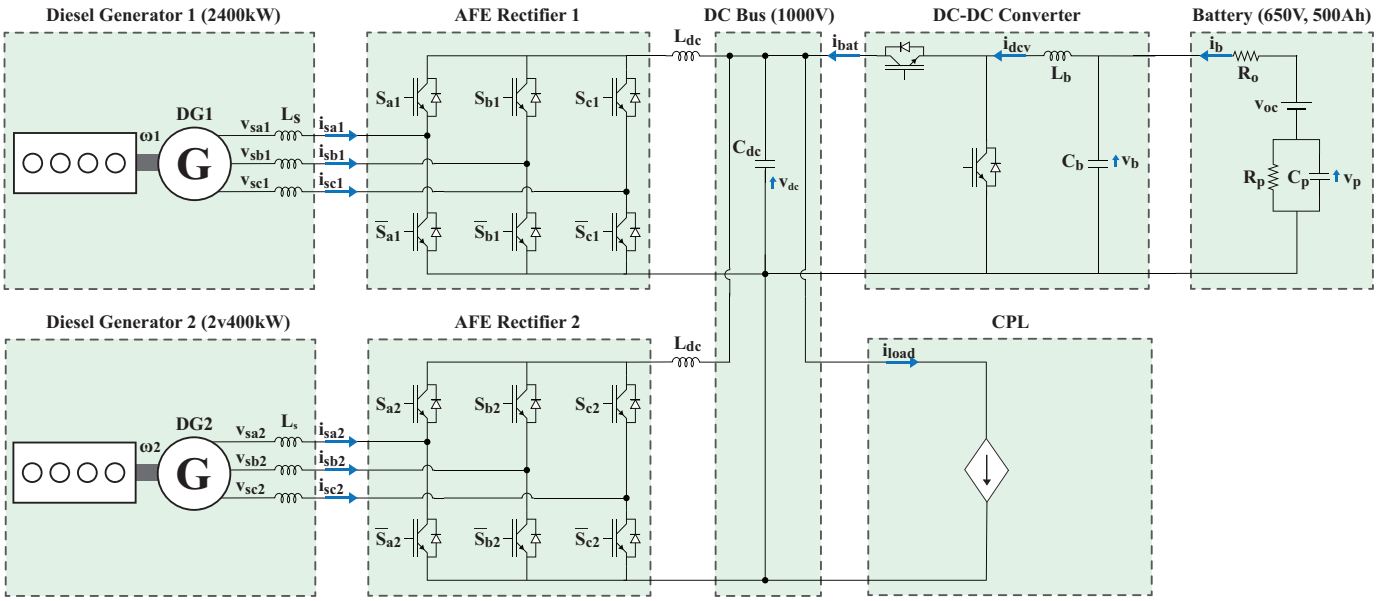

Fig. 2: Schematic diagram of the shipboard DC power system for the study.

- Generator models (3^{rd} order model):

The 3^{rd} order (The One-Axis or Flux-Decay) model is used for the generator in direct and quadrature (dq) axis [31], [32]. This reduced-model neglects factors that are not critical to the system-level analysis such as rotor body eddy currents, the effects of the damper windings and the d-axis transient emf. However, the model can still represent the effect of the excitation voltage from AVR so that the dynamics of AVR controller can be included in the system. As a result, the model is presented as:

$$\dot{\delta}_i = \omega_i - \omega_i^* \tag{4}$$

$$\dot{\omega}_i = \frac{1}{2H_i}(T_{m,i} - T_{e,i} - D_i\omega_i) \tag{5}$$

$$\dot{e}'_{q,i} = \frac{1}{T'_{do,i}}\left(E_{f,i} - e'_{q,i} - \frac{(x_{gd,i} - x'_{gd,i})}{I_{nom,i}} i_{sd,i}\right) \tag{6}$$

$$\dot{X}_{avr,i} = v^*_{s,i} - \sqrt{v^2_{sd,i} + v^2_{sq,i}} \tag{7}$$

$$E_{f,i} = k_{p,avr_i}(v^*_{s,i} - \sqrt{v^2_{sd,i} + v^2_{sq,i}}) + k_{i,avr_i}X_{avr,i} \tag{8}$$

$$T_{e,i} = \frac{e'_{q,i} i_{sq,i}}{\omega_i I_{nom,i}} + \frac{(x_{gq,i} - x'_{gd,i}) i_{sd,i} i_{sq,i}}{\omega_i I^2_{nom,i}} \tag{9}$$

$$v_{sd,i} = \frac{x_{gq,i}}{I_{nom,i}} i_{sq,i} \tag{10}$$

$$v_{sq,i} = e'_{q,i} - \frac{x'_{gd,i}}{I_{nom,i}} i_{sd,i} \tag{11}$$

where δ_i [pu] is the relative load angle from the reference speed, H_i [s] is the inertia constant ($H = \frac{J\Omega^2}{2S}$, where J $[kg \cdot m^2]$ is the moment of inertia of the diesel engine and generator, Ω [rad/s] is the base angular velocity and S [VA] is the three-phase rating of the generator), $T_{e,i}$ [pu] is the electrical torque, D_i [pu] is the damping coefficient, $e'_{q,i}$ [pu] is the q-axis transient emf, $T'_{do,i}$ [pu] is the direct axis transient time constant, $E_{f,i}$ [pu] is the field voltage controlled by AVR represented as a PI controller with gains (k_{p,avr_i} and k_{i,avr_i}), $x_{gd,i}$ [pu] is the d-axis reactance of the generator, $x'_{gd,i}$ [pu] is the d-axis transient reactance of the generator, $I_{nom,i}$ [A] is the nominal current to convert the current value to per unit value, $X_{avr,i}$ [pu] is the voltage error dynamics for AVR, $v^*_{s,i}$ [pu] is the AC voltage reference, $v_{s,i}$ [pu] and $i_{s,i}$ [A] are the voltage and current in dq-axis ($v_{sd,i}$, $v_{sq,i}$, $i_{sd,i}$ and $i_{sq,i}$ respectively) and $x_{gq,i}$ [pu] is the q-axis reactance of the generator.

B. AC-DC Interface: AFE rectifiers and DC-Bus

The AFE rectifiers are modeled based on averaged model with their PI controllers in d- and q-axis represented with $Z^*_{d,i}$ [V] and $Z^*_{q,i}$ [V] respectively [33]. The PI controllers for the current and voltage on AFE1 and AFE2 are shown control blocks of Fig. 3. Furthermore, the DC bus integrates AC subsystem, DC subsystem and the load through a capacitor bank (C_{dc}) which also includes the individual capacitors in each component. The resulting model is presented as:

$$\dot{i}_{sd,i} = \frac{1}{L_{s,i}} Z^*_{d,i} = \frac{1}{L_{s,i}}(k_{pd,i}(i^*_{sd,i} - i_{sd,i}) + k_{id,i}X_{d,i}) \tag{12}$$

$$\dot{i}_{sq,i} = \frac{1}{L_{s,i}} Z^*_{q,i} = \frac{1}{L_{s,i}}\left(k_{pq,i}(i^*_{sq,i} - i_{sq,i}) + k_{iq,i}X_{q,i}\right) \tag{13}$$

$$\dot{X}_{e,i} = v^*_{ls,i} - v_{dc} \tag{14}$$

$$\dot{X}_{d,i} = i^*_{sd,i} - i_{sd,i} \tag{15}$$

$$\dot{X}_{q,i} = i^*_{sq,i} - i_{sq,i} \tag{16}$$

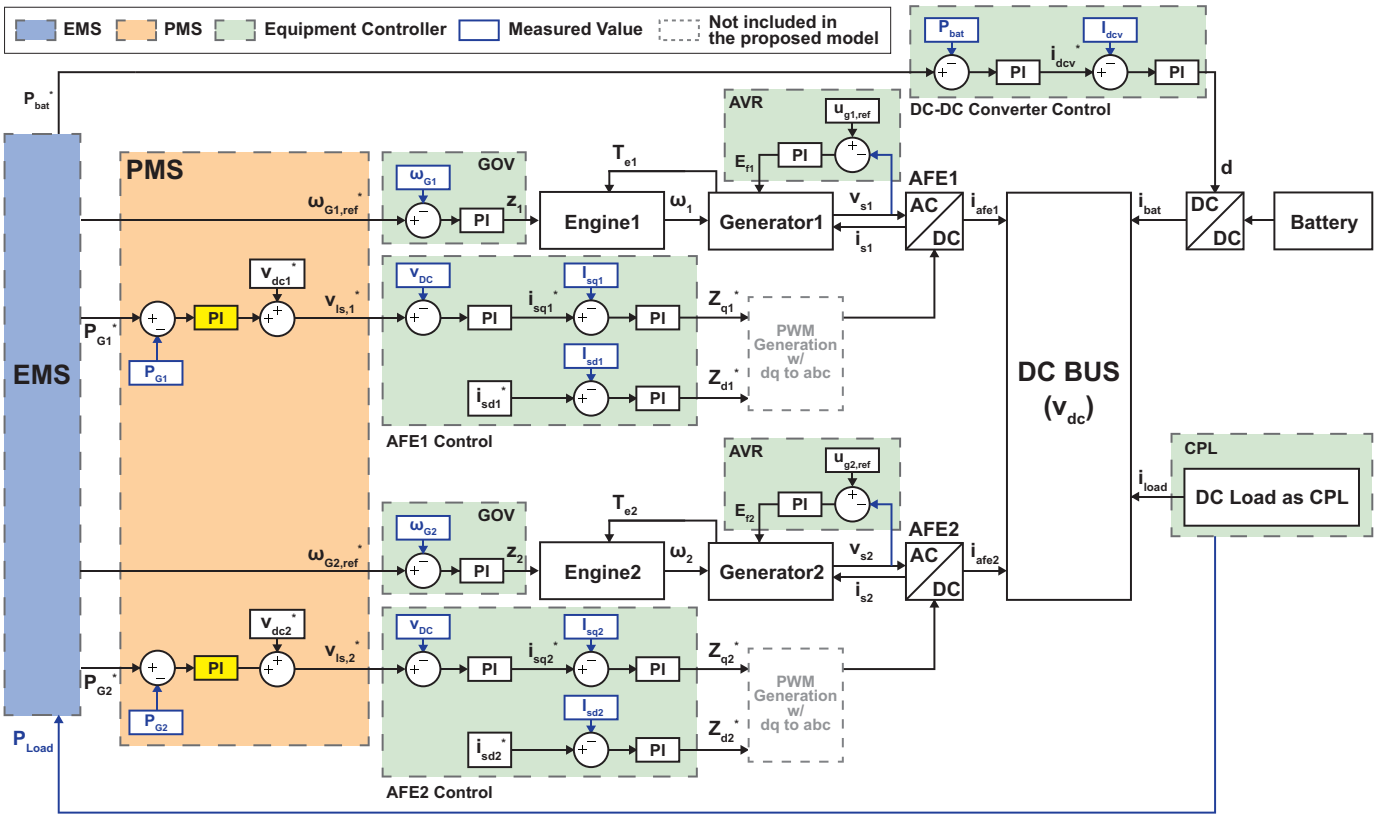

Fig. 3: Control Scheme of the shipboard DC power system for the study (PI controller in the yellow block will be evaluated further with stability analysis and time-domain simulations).

$$\dot{v}_{dc} = \frac{1}{C_{dc}}\left(\frac{\sum_{i=1}^{2} P_{afe,i} + P_{bat} - P_{load}}{v_{dc}}\right) = \frac{1}{C_{dc}v_{dc}}\sum_{i=1}^{2} P_{afe,i} + \frac{i_{bat}}{C_{dc}} - \frac{P_{load}}{C_{dc}v_{dc}} \tag{17}$$

$$P_{afe,i} = \frac{3}{2}\Big(i_{sd,i}(V_{nom,i}v_{sd,i} - Z^*_{d,i}) + i_{sq,i}(V_{nom,i}v_{sq,i} - Z^*_{q,i})\Big) \tag{18}$$

$$i^*_{sq,i} = k_{pe,i}(v^*_{ls,i} - v_{dc}) + k_{ie,i}X_{e,i} \tag{19}$$

$$Z^*_{d,i} = k_{pd,i}(i^*_{sd,i} - i_{sd,i}) + k_{id,i}X_{d,i} \tag{20}$$

$$Z^*_{q,i} = k_{pq,i}(i^*_{sq,i} - i_{sq,i}) + k_{iq,i}X_{q,i} \tag{21}$$

where $X_{e,i}$ [V] is the DC-bus voltage (v_{dc} [V]) error dynamics for a PI controller with gains ($k_{pe,i}$ and $k_{ie,i}$) based on the reference of $v^*_{ls,i}$ [V] that is defined in (33) in PMS section, $X_{d,i}$ [A] is the d-axis current error dynamics with $k_{pd,i}$ and $k_{id,i}$ as the controller gains (the reference current $i^*_{sd,i}$ [A] is kept to zero), $X_{q,i}$ [A] is the q-axis current error dynamics with $k_{pq,i}$ and $k_{iq,i}$ as the controller gains (the reference current $i^*_{sq,i}$ [A] is calculated from the outer loop of AFE voltage control), $P_{afe,i}$ [W] is the output power from the AFEs calculated by (18), P_{bat} [W] is the DC-DC converter output power for the battery that can be calculated by $v_{dc}i_{bat}$, P_{load} [W] is the aggregated load from tightly regulated power converters such as variable speed drives (VSDs) and V_{nom} [V] is the conversion factor to convert per-unit value to voltage.

C. DC subsystem: DC-DC converter and battery system

The DC sub-system consists of a half-bridge bidirectional DC-DC converter with a battery bank which is represented by its Thévenin circuit model in Fig. 2. From the DC subsystem model, P_{bat} will be derived and applied to (17). Compared to Rint model that only includes an open circuit voltage (v_{oc}) and internal resistance (R_o), Thévenin model can represent the dynamic response of the battery to the instantaneous load [34]. However, v_{oc} is assumed to be constant and the self-discharging resistance is ignored for this study. The design of DC-DC converter control can be found in Fig. 3 as a cascade control using PI controllers. Therefore, the resulting model becomes:

$$\dot{i}_{dcv} = \frac{v_b}{L_b} - d\frac{v_{dc}}{L_b} \tag{22}$$

$$\dot{v}_b = \frac{1}{C_b}i_b - \frac{1}{C_b}i_{dcv} \tag{23}$$

$$\dot{v}_p = \frac{1}{C_p}i_b - \frac{1}{C_pR_p}v_p \tag{24}$$

$$\dot{X}_{bp} = P^*_{bat} - P_{bat} = P^*_{bat} - v_b i_{dcv} \tag{25}$$

$$\dot{X}_{bi} = i_{dcv} - i^*_{dcv} \tag{26}$$

$$d = k_{p,bi}(i_{dcv} - i^*_{dcv}) + k_{i,bi}X_{bi} \tag{27}$$

$$i^*_{dcv} = k_{p,bp}(P^*_{bat} - P_{bat}) + k_{i,bp}X_{bp} \tag{28}$$

$$i_b = \frac{v_p + v_{oc} - v_b}{R_o} \tag{29}$$

$$i_{bat} = di_{dcv} \tag{30}$$

$$SOC = SOC_0 - \frac{1}{k_b Q_b}\int_0^t i_b dt \tag{31}$$

where, i_{dcv} [A] is the current through the inductor in the converter, v_b [V] is the output voltage of the battery, d [pu] is the duty cycle of a switch based on the buck mode operation (battery charging) while $1-d$ [pu] is assigned to the other switch (both duty cycles are saturated between 0 and 1), i_b [A] is the battery output current, v_p [V] is the transient voltage in the battery through the capacitor (C_p), X_{bp} [W] is the power error dynamics for the power control loop (outer) of the DC-DC converter with a PI controller ($k_{p,bp}$ and $k_{i,bp}$) to generate the current reference (i^*_{dcv}) for the current loop, X_{bi} [A] is the current error dynamics for the current control loop (inner) of the DC-DC converter with a PI controller ($k_{p,bi}$ and $k_{i,bi}$) to calculate the duty cycle, P^*_{bat} [W] is the battery power reference for the DC-DC converter and P_{bat} [W] is the measured battery power that can be calculated as $v_b i_{dcv}$. Lastly, the battery output current is integrated over time to calculate the change in the state of charge (SOC) of the battery from its initial charge (SOC_0) with a conversion factor of k_b (from second to hour) and Q_b [Ah] is the rated capacity of the battery.

Optionally, if the battery takes part in the load sharing same as the AFE rectifiers, the power control loop for the DC-DC converter in (25) and (28) should be replaced with a voltage loop having its reference ($v^*_{ls,b}$) followed by a modified PMS design. Similarly, it is also useful to have a voltage control loop (outer) in the peak shaving operation. Otherwise, the required power from the battery should be calculated from EMS and delivered to the converter controller as presented.

D. Power Management System (PMS) with Enhanced Power Control Performance

The PMS architecture and model is presented and is tuned for equal and unequal load sharing. To increase the power set-point tracking performance and to make DC voltage more stable, the DC voltage reference in the AFE's voltage control loop (outer) as seen in (14) and (19) is derived in order to assign different values of the voltage reference so that each AFE can be operated more effectively under both equal and unequal load sharing condition. This control method is integrated with inverse voltage droop control as seen in PMS and AFE control blocks in Fig. 3. The resulting equations are presented below:

$$\dot{P}_{err,i} = P_{ref,i} - P_i \approx P_{ref,i} - \frac{3V_{nom,i}}{2} v_{sq,i} i_{sq,i} \tag{32}$$

$$v^*_{ls,i} = v^*_{dc,i} + k_{p,V_i}(P_{ref,i} - P_i) + k_{i,V_i} P_{err,i} \tag{33}$$

$$\begin{aligned} P_i &= V_{nom,i}\frac{3}{2}(v_{sd,i} i_{sd,i} + v_{sq,i} i_{sq,i}) \\ &\approx V_{nom,i}\frac{3}{2} v_{sq,i} i_{sq,i} \end{aligned} \tag{34}$$

where P_i [W] is the output power of the AFE (ith) that can be calculated by assuming the d-axis current ($i_{sd,i}$ equals to zero. Then, the deviation of the AFE output power from its reference value (delivered from EMS) is calculated as error dynamics of $P_{err,i}$ [W]. This error term is then compensated by a PI regulator with control coefficients k_{p,V_i} and k_{i,V_i}. $v^*_{dc,i}$ [V] is the reference DC voltage that can be produced by a droop/isochronous load sharing. (32) shows how the voltage set-point is generated in a general form. In this study, v^*_{dc} is set to be constant meaning that the droop gain is equal to zero. In addition, the error is compensated by the term (32). For the purpose of comparison, the conventional droop/isochronous control method is also presented to calculate v^*_{dc} as:

$$v^*_{ls,i} = v^*_{dc,i} = v_{0,i} - droop_i \times P_i \tag{35}$$

where $v_{0,i}$ is the no-load voltage, $droop_i$ is the droop gain. Both parameters should be decided at every sampling time of P^*_i. In isochronous control mode, $droop_i$ is equal to zero, meaning that the voltage set-point is always constant. In the conventional droop or isochronous control, (32)-(33) are not used, meaning that a steady-state error can be observed.

(a) Linearized **A** matrix for the entire system

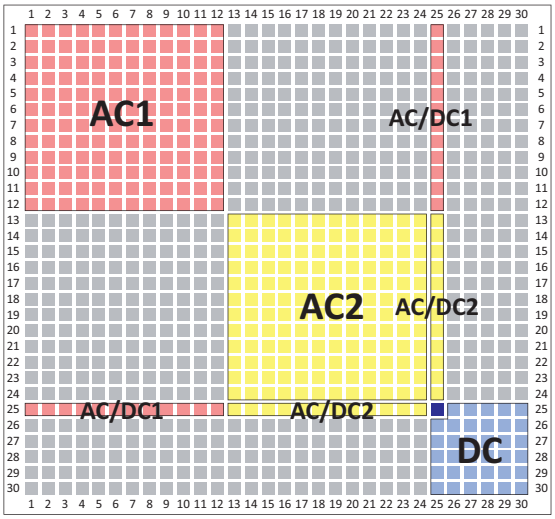

(b) Linearized **A** matrix for the modularized systems

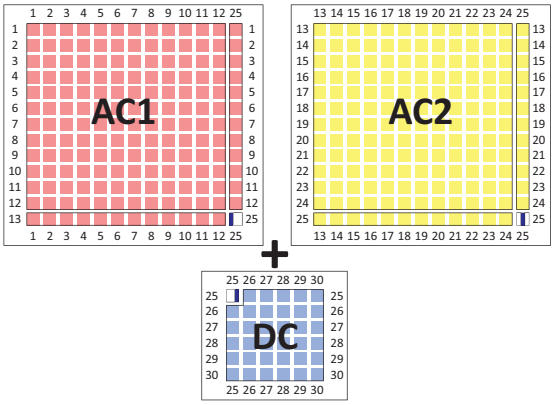

Fig. 4: Analysis of A matrix of the linearized system

III. Small-Signal Stability Analysis and Control Design

Here, a state-space model of the total system (sub-systems and controllers) is developed based on the presented methodology in Section II. The eigenvalues are then derived and used for the stability analysis of the entire system. The control tuning and the comparison with the conventional controller are also presented in this section. The equations from (1) to (34) are then gathered to become a full set of the system model in a form of a nonlinear system ($\dot{\mathbf{x}} = f(\mathbf{x}, \mathbf{u})$). For the further analysis of the system, the model is linearized at an equilibrium point ($\mathbf{x}_o$ and $\mathbf{u}_o$) to evaluate the parameters if they ensure the system stability based on the eigenvalue analysis with root locus plots and the results of the analysis are validated by time domain simulations. The linearized system is given as:

$$\mathbf{\Delta\dot{x}} = \mathbf{A(x_o, u_o)\Delta x + B(x_o, u_o)\Delta u} \tag{36}$$

where, the states are $\mathbf{x}$ = [$P_{err,1}$ $T_{m,1}$ $X_{gov,1}$ δ_1 ω_1 $e'_{q,1}$ $X_{avr,1}$ $i_{sd,1}$ $i_{sq,1}$ $X_{e,1}$ $X_{d,1}$ $X_{q,1}$ $P_{err,2}$ $T_{m,2}$ $X_{gov,2}$ δ_2 ω_2 $e'_{q,2}$ $X_{avr,2}$ $i_{sd,2}$ $i_{sq,2}$ $X_{e,2}$ $X_{d,2}$ $X_{q,2}$ v_{dc} i_{dcv} v_b v_p X_{bp} X_{bi}]^T and the inputs are $\mathbf{u}$ = [$P_{ref,1}$ ω_1^* $v_{s,1}^*$ $i_{sd,1}^*$ $P_{ref,2}$ ω_2^* $v_{s,2}^*$ $i_{sd,2}^*$ v_{dc}^* P_{bat}^* P_{load}]^T.

With $A(\mathbf{x}_o, \mathbf{u}_o)$ matrix, the stability analysis of the system can be carried out with the eigenvalues. Before the analysis, it is useful to understand how the matrix is organized first, as shown in Fig. 4(a) for indication of the null matrices (gray boxes) and Fig. 4(b) for further modularization of the system.

In Fig. 4(a), the figure shows how its sub-matrices can be found respectively. The element in the navy box represents a Δv_{dc}-related components, and this component functions as a bridge between AC subsystems and DC subsystems, so the entire matrix can be decomposed into several independent systems by distributing Δv_{dc}-related component as shown in Fig. 4(b) (colored with navy partially). From (37) where $\mathbf{R}_1^T$ and $\mathbf{R}_2^T$ represents the remaining terms for reduced number of states ($\mathbf{x}_d$) and inputs ($\mathbf{u}_d$), we can understand the equation (37) that the first two terms with P_{load} and $P_{afe,i}$ are the contributions from the load balance and the last term with $i_{sq,i}$ is the contribution for compensating current to control the DC voltage. By assigning each contribution in (37) to each subsystem, the system can be finally modularized so that it is possible to calculate each module's stability properties and to design each module's elements because these modules are separated components in the real installation.

A. Eigenvalue-based Stability Analysis and Time-domain Simulation

The system is analyzed based on the system parameters defined in Table. II with different PMS control parameters (k_{p,V_i} and k_{i,V_i}). In Fig. 5, five eigenvalues that are mostly affected by the control parameter changes are found as all other eigenvalues are placed in left-half plane (LHP) satisfying the stability criterion. Noting that the eigenvalue 4 and 5 are scaled down, eigenvalue 2, 3 and 5 becomes more stable as k_{p,V_i} increases as shown in Fig. 5(a,c,e). The effect of the increasing value of eigenvalue 4 can be ignored since it has already a big enough negative value. However, the eigenvalue 5 which has the lowest damping can be only moved towards negative by increasing k_{i,V_i}.

For the verification of the root-locus analysis, the time domain verification is done as shown in Fig. 6 based on the maximum load ramp-up condition which is 1200kW increase (50% of the rated capacity) within 10s for No.2 genset. When

$$\Delta\dot{v}_{dc} = \left| \frac{1}{C_{dc}v_{dc}} \left(\frac{P_{load}}{v_{dc}} - \sum_{i=1}^{2} \left(\frac{P_{afe,i}}{v_{dc}} - \frac{3}{2} k_{pq,i} k_{pe,i} i_{sq,i} \right) \right) \right|_{\mathbf{x_o}, \mathbf{u_o}} \Delta v_{dc} + \mathbf{R_1}^T \Delta \mathbf{x}_d + \mathbf{R_2}^T \Delta \mathbf{u}_d \tag{37}$$

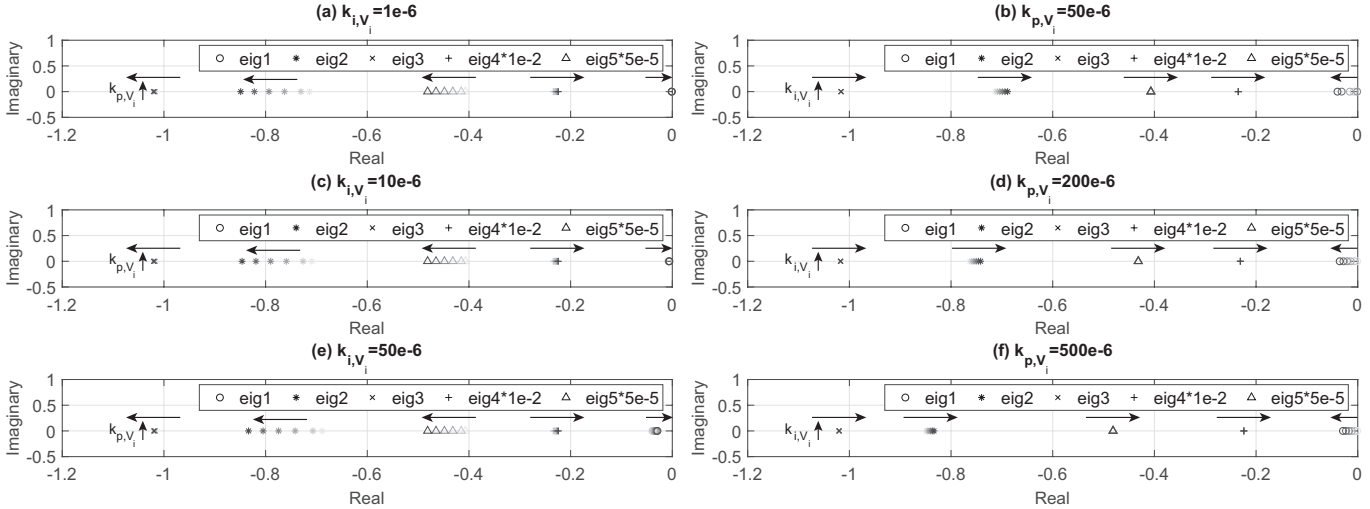

Fig. 5: Root-locus of eigenvalues for varying PMS PI controller parameters where $P_{ref,i} = P_i = 1600kW$. (a,c,e) k_{p,V_i} sweep with k_{i,V_i} constant (b,d,f) k_{i,V_i} sweep with k_{p,V_i} constant.

This article has been accepted for publication in a future issue of this journal, but has not been fully edited. Content may change prior to final publication. Citation information: DOI 10.1109/TTE.2021.3119231, IEEE Transactions on Transportation Electrification

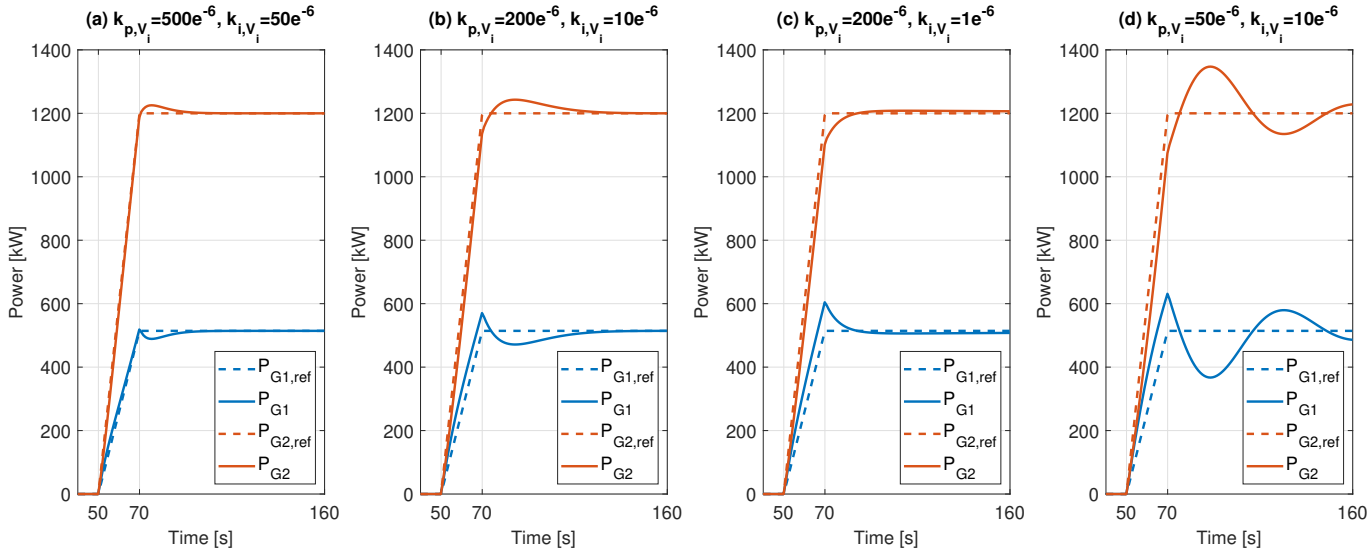

Fig. 6: Time-domain verification of PMS controller tuning with different k_{p,V_i} and k_{i,V_i}

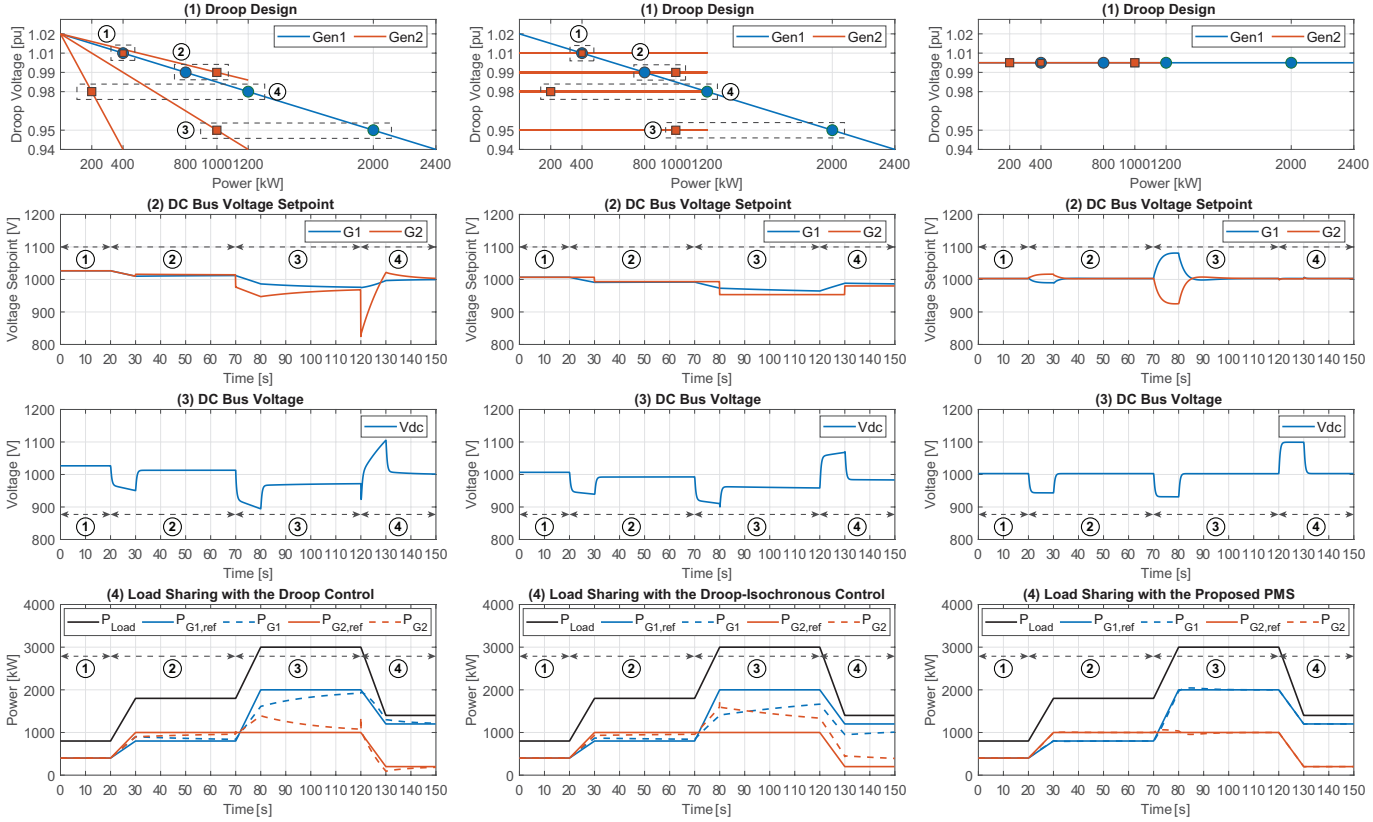

(a) Droop control only (b) Droop and Isochronous control (c) Proposed control

Fig. 7: The comparison of PMS between the proposed method and the conventional methods (droop and isochronous control) for Load Case1: 800kW (G1:400/G2:400kW), Case2: 1800kW (G1:800/G2:1000kW), Case3: 3000kW (G1:2000/G2:1000kW), Case4: 1400kW (G1:1200/G2:200kW). (1) Droop design for four different load-sharing scenarios for $v^*_{dc,i}$ (2) Resulting DC bus voltage set-points for $v^*_{ls,i}$ (3) Resulting DC bus voltage (4) Power set-point tracking performance.

Fig. 6(b) and Fig. 6(d) are compared, the effect of k_{p,V_i} can be verified that higher k_{p,V_i} can provide more damping in the power output. Similarly, when Fig. 6(b) and Fig. 6(c) are compared, it can be seen that higher k_{i,V_i} can eliminate a steady-state bias that is the slowest dynamics. Finally, the final tuning parameters are found as presented in Fig. 6(a) to achieve the fastest response in the output power.

TABLE I: The comparison of PMS between the proposed method and the conventional methods based on Fig.7

	Droop control (conventional)	Droop+Isochronous (conventional)	PI control (proposed)
Load sharing method	G1 : Fixed droop curve (primary), G2 : Droop gain to be updated at every new power reference (secondary)	G1 : Fixed droop curve (primary), G2 : Droop gain to be updated at every new power reference (secondary)	G1, G2 : Automatic by PI controller, no designated main or secondary power source
Transient load handling method	Depending on the droop gain (a machine with a droop gain closer to zero handles the transient loads faster)	A machine with isochronous mode can always handle the transient loads faster	Both machines handle the transient loads proportionally
Voltage error (rms)	37.03 V	37.49 V	33.68 V
Power error (rms)	P1 : 132.04 kW P2 : 132.42 kW	P1 : 276.47 kW P2 : 276.69 kW	P1 : 16.78 kW P2 : 16.77 kW

B. Control Performance Comparison

For further evaluation, the given PMS is compared with the conventional load sharing methods such as DC voltage droop and isochronous control [8]. In the conventional load sharing methods, the voltage set-point is derived from (35). Three different cases are compared as droop only, droop & isochronous, and the proposed method. The results are summarized in Fig. 7. It is to be noted that only isochronous mode is not considered because it is not a possible operation scenario for the designated load sharing conditions. Each droop design is shown in Fig. 7(a1), (b1) and (c1). For droop control only, the droop curve of genset 1 is fixed and the droop curve of genset 2 changes with the new power set-points. For droop and isochronous control, the droop curve of genset 1 remains the same as the previous case but the droop curve of genset 2 is constant to implement the isochronous operation until the new power set-point is given. Then, the droop curve jumps to another constant point. Finally, for the proposed control, the droop curve can remain constant regardless of any power levels since the PI controllers can handle the load sharing. In Fig. 7(c2), the DC voltage reference for load sharing ($v^*_{ls,i}$) to the AFEs can remain around v^*_{dc}. As a result, the resulting DC voltage references can be symmetrical with v^*_{dc} as a centerline, which can help to maintain the DC voltage constant at its set-point instead of decreasing the voltage in case of the conventional control as shown in Fig. 7(a2) and (b2). These sudden voltage changes induced by the droop method become especially greater because the droop gain should also change rapidly when the load changes steeply from the load case 3 to 4 at 120s. For the conventional control methods, the no-load voltage and the droop gain should be calculated at every new power set-point to satisfy the dynamic changes of load sharing conditions defined by EMS. However, with an additional PI controller, the procedure to calculate the reference voltage to the AFEs ($v^*_{ls,i}$) can be much more simplified and automated and further voltage restoration is not necessary.

Furthermore, the proposed method improves the power set-point tracking performance as shown in Fig. 7(c4) compared to 7(a4) and (b4). The recent development of intelligent EMS has been introduced in the marine power system to reduce fuel consumption and its associated emissions. Then, it is very important in the EMS performance that EMS updates new power set-points as fast as possible to cope with the load variations. However, with the conventional methods, they show a slower response to follow the power references. Therefore, the performance will be even worse with the lower updating frequency. The load sharing and transient load handling methods for each case are summarized in Table I including RMS errors in voltage and power calculated from the results of Fig. 7. The errors show the improved performance both in voltage and power control in the proposed control method. The worst power performance is observed in the mixed droop and isochronous control because the genset 2 is prone to act as a swing machine to the transient loads in addition to its designated power set-point. The effect of adding isochronous mode is clearly seen at the beginning of load case 3.

To sum up, the (unequal) load sharing performance can be decided by the voltage difference between the power

TABLE II: Main Parameters of the proposed DC SPS model

Parameter	Value
Diesel Engine and Generator	
Diesel engine rated power	$P_{gen,i}$ = 2400kW
Diesel engine time constant	$T_{de,i}$ = 5s
Engine speed reference	ω^*_i = 1pu (720 rpm)
Governor PI controller gains	k_{p,gov_i} = 3, k_{i,gov_i} = 1
The genset inertia constant	H_i = 1.148s
Damping coefficient	D_i = 0.05pu
d-axis transient time constant	T'_{do} = 0.995s
d-axis reactance	$x_{gd,i}$ = 1.379pu
d-axis transient reactance	$x'_{gd,i}$ = 0.23pu
q-axis reactance	$x_{gq,i}$ = 0.873pu
AVR controller gains	k_{p,avr_i} = 1e^{-2},k$_{i,avr_i}$ = 1e^{-3}
AFE rectifier	
Line inductance	$L_{s,i}$ = 100μH
DC bus capacitance	C_{dc} = 50mF
d-axis current reference	$i^*_{sd,i}$ = 0A
AFE controller (voltage loop)	$k_{pe,i}$ = 0.5, $k_{ie,i}$ = 1
AFE controller (q-current loop)	$k_{pq,i}$ = 2, $k_{iq,i}$ = 1
AFE controller (d-current loop)	$k_{pd,i}$ = 1e^{-2},k$_{id,i}$ = 1e^{-2}
DC-DC converter	
Inductor	L_b = 40mH
Capacitor	C_b = 1mF
Battery	
Open circuit voltage	v_{oc} = 650V
Internal resistance	R_o = 50mΩ
RC parallel network	R_p = 13mΩ,C$_p$ = 14300F
Initial state of charge	SOC_0 = 0.9pu
Battery capacity with conversion factor	Q_b = 500Ah, k_b = 3600s
Controller (power loop)	$k_{p,bp}$ = 0.5, $k_{i,bp}$ = 5
Controller (current loop)	$k_{p,bi}$ = 0.01, $k_{i,bi}$ = 0.1
PMS	
PI controller gains	k_{p,V_i} = 500e^{-6},k$_{i,V_i}$ = 50e^{-6}
DC bus voltage reference (isochronous)	v^*_{dc} = 1000V

sources. If it is possible to shape the voltage symmetrical as proposed, the voltage difference between the two gensets can be maximized so that the load sharing performance can be improved while keeping the voltage change as low as possible. On the other hand, the voltage difference for the droop and isochronous control cannot be as big as the proposed method since they have the same sign of droop gain (or zero in case of the isochronous control). Then, the load sharing performance also decreases resulting in higher voltage fluctuations.

IV. Simulation Results and Experimental Validation

To verify the performance of the proposed modeling approach and control strategy, simulation models are established in MATLAB/Simulink and the dynamic analysis of the system is conducted with the model parameters given in Table II. Simulations are carried out with four different operation scenarios under the unequal load sharing profile calculated for each genset by an optimization-based EMS (based on mixed-integer linear programming) for a real ferry operation. As [35] suggests, it is important for the EMS to consider not only fuel consumption reduction but also the synchronization of the running hours of the gensets. Therefore, the EMS produces power set-points considering these two objectives while the battery power set-points are generated in order to stabilize the voltage and load fluctuations on the gensets. In addition, the load leveling operation of the battery is presented in the last simulation case. It is to be noted that the main control of bus voltage is carried out by the gensets through AFE rectifiers in the shipboard hybrid power systems since the battery cannot supply all the massive propulsion loads for a long cruising range due to its limited energy capacity. Therefore, in this study, it is proposed to use the battery as a grid supporting component. The first simulation is carried out with only two gensets to verify the unequal load sharing performance and its effect on the DC bus voltage. For the second and third

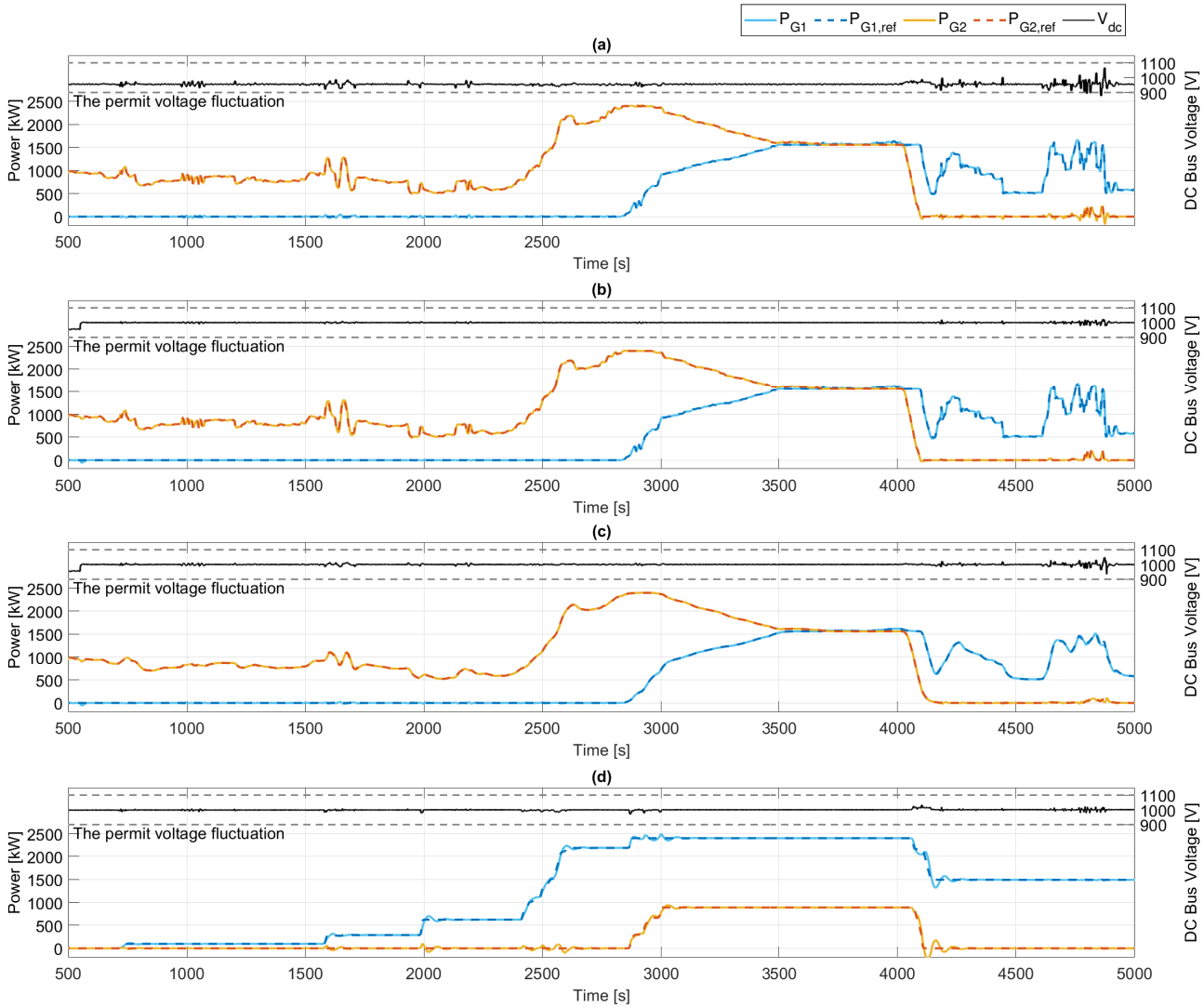

Fig. 8: The simulation results. (a) Load sharing without battery operation (b) Load sharing with battery operation for voltage compensation (c) Load sharing with battery operation for load smoothing (d) Load sharing between all the gensets and the battery including load smoothing operation (the permit DC bus voltage fluctuation is given by 10% of the nominal voltage)

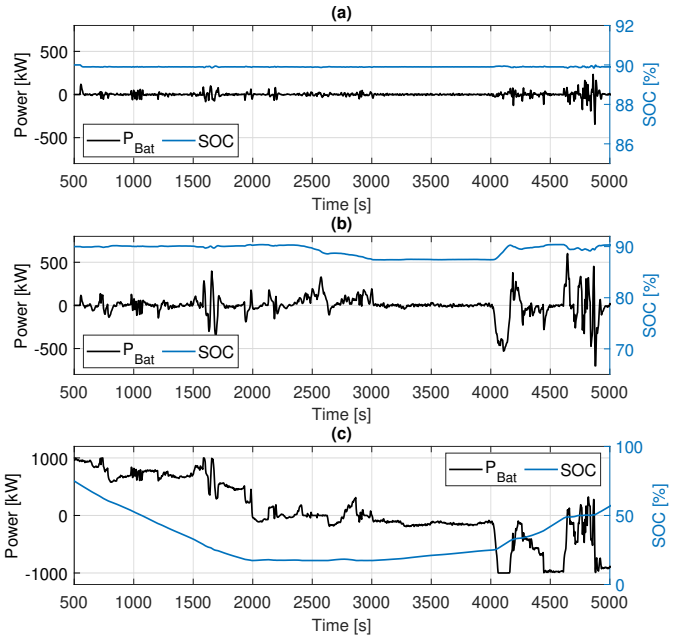

Fig. 9: Battery output power and SOC variation for different mode of battery operations. (a) Battery operation for voltage compensation (b) Battery operation for load smoothing (c) Battery operation for load leveling and smoothing

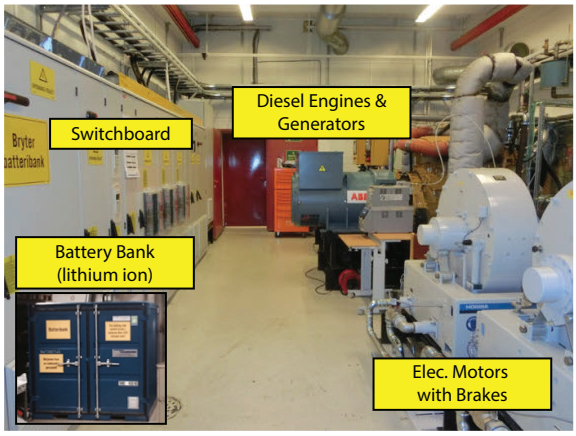

Fig. 10: Laboratory facility in Hybrid Power Lab at NTNU.

TABLE III: Specifications of the Test-bed in HPL

Equipment	Specifications
Diesel Generator	400 kVA, 4 poles, 1200-1750 rpm
Battery Bank	Li-ion, 65 Ah, 346 V
Electric motor loads	160 kW, 1,015 nm at 1500 rpm
DC Bus Voltage	540 V

operations, the battery is utilized in order to stabilize the DC voltage and to assign slow dynamics to the genset operations. Lastly, in the last operation, the load is shared actively among the gensets and the battery while the voltage stabilization function is still remained. The simulation results are given in Fig. 8 and Fig. 9.

The results show that the fluctuations in all cases fulfill the requirement, but it should be noted that these are the output voltages from the control plant. It should be maintained as low as possible since the fluctuation becomes greater in the actual voltage due to the system response, switching effect, etc.

For the case of without battery operation in Fig. 8(a), the power outputs from each genset show good power tracking performance (continuous lines) of their set-points (dashed lines), but the DC bus voltage should be sacrificed as it shows higher fluctuations when the load is changing rapidly. The case of Fig. 8(b) aims for the battery to minimize the voltage fluctuations only, while the case of Fig. 8(c) aims for the battery to handle both the voltage fluctuations and load smoothing operation to assign a slow-varying load to the gensets. This is why Fig. 8(c) and (d) show more fluctuations compared to Fig. 8(b) since two missions conflict in assigning the battery power (i.e. sacrificing the voltage). The case of Fig. 8(d) shows the maximum utilization of the battery energy to reduce fuel consumption. Therefore, each genset produces power differently from the other cases. Even though the power tracking performance is slightly less than the other cases during the transient conditions, the result shows the unequal load sharing can be still done with an acceptable accuracy under the proposed control method.

For the battery operations, the effort to minimize the DC bus voltage fluctuation is implemented by replacing the power control loop with the voltage control loop to generate battery current references (i^*_{dcv}) in (25) and (28), and the result is shown in Fig. 9(a) for its power output and SOC. Additionally, load smoothing operation by the battery is implemented in order to minimize load fluctuations to the gensets and to improve the genset's transient responses, and the result is presented in Fig. 9(b) for its power output and SOC. It is noted that more energy from the battery system is utilized to smoothen the genset output power in addition to the voltage compensation mission. When the battery is used as a load leveling (sharing a significant amount of load) in Fig. 9(c), the change of SOC is larger than the other cases. To sum up, the results show that the proposed model framework and control method can be easily implemented with any type of ship operating conditions within acceptable accuracy.

The proposed model is validated with the experimental results from the hybrid power lab (HPL) at Norwegian University of Science and Technology (NTNU) [36]. The experiment is implemented with one set of diesel engine and generator with rectifier and a battery system which is interfaced to the DC bus by a DC-DC converter as presented in Fig. 10. As a load, one electric motor with a water-cooled brake is connected to a variable speed drive (VSD) and VSD follows designated speed and torque references to emulate the propulsion load of the ship. The detailed specifications of the lab equipment are described in Table III.

The experimental data based on a predefined load profile from the HPL is collected with engine speed, voltage, current, and power of each component as well as voltage set-points from the PMS. Then, assigning the same power to the AFE rectifier and DC-DC converter in the two simulation models (the proposed model and the Simscape model in Matlab/Simulink) for the verification with the same high-

This article has been accepted for publication in a future issue of this journal, but has not been fully edited. Content may change prior to final publication. Citation information: DOI 10.1109/TTE.2021.3119231, IEEE Transactions on Transportation Electrification

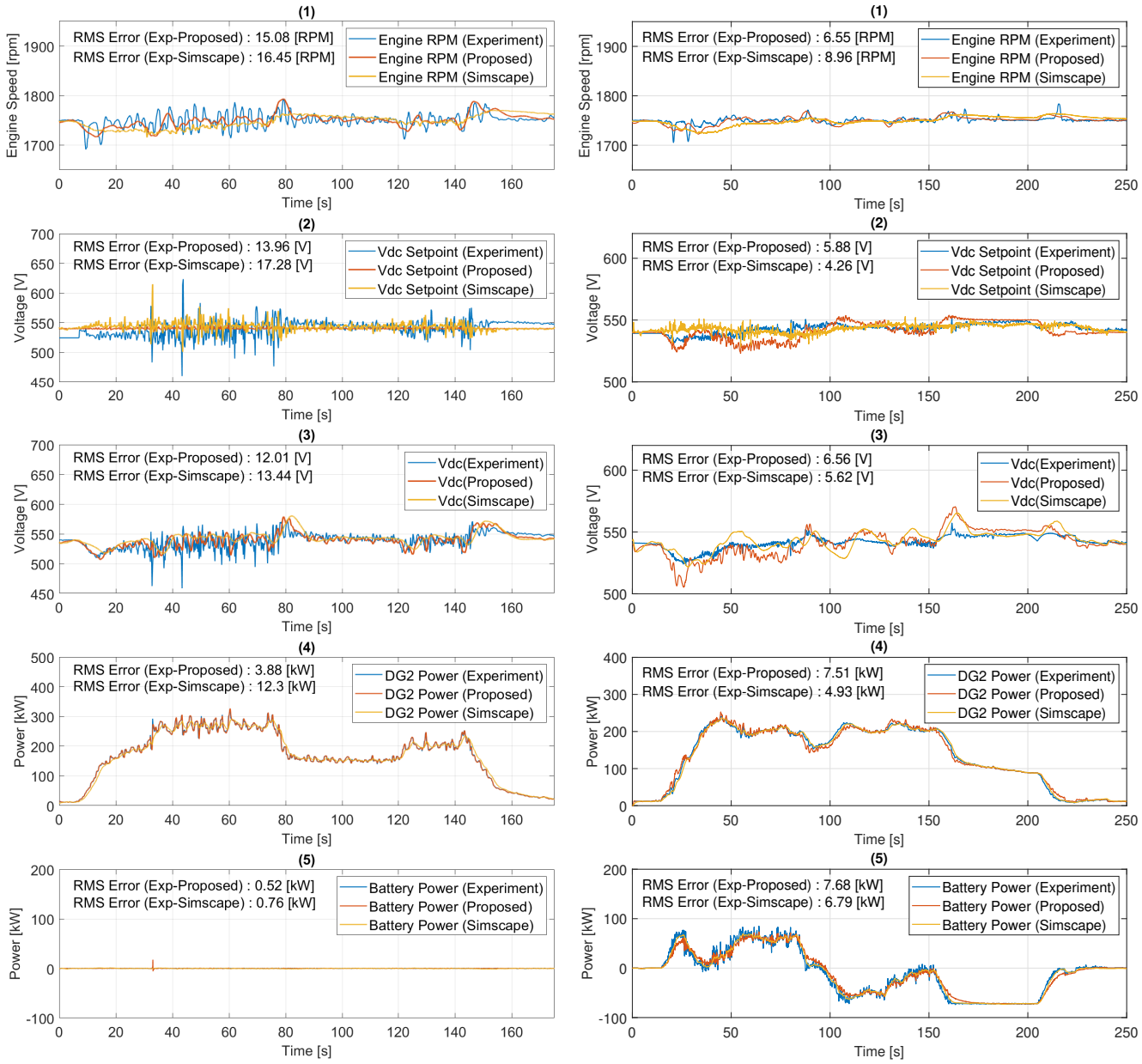

(a) Without battery operation (b) With battery operation

Fig. 11: The result of experimental validations compared to the simulation results (the proposed model and the Simscape model). (1) Engine Speed (2) DC bus voltage set-point (3) DC bus voltage (4) DG2 output power (5) Battery output power

level PMS control strategy, the simulation results of engine speed, DC bus voltage, and its set-point are compared with the collected experimental data as seen in Fig. 11. The Simscape model represents a more detailed model that replicates the HPL including the switching effect of the DC-DC converter. Lastly, the RMS error rates are calculated to show deviations in each result between the experiment - the proposed model simulation results and between the experiment - the Simscape model simulation results. Then, two cases of the experiment are implemented as with battery and without battery operation as given in Fig. 11.

In Fig. 11(a), the proposed model shows a better accuracy compared to the Simscape model. When the engine speed and the DC bus voltage are compared, the proposed model outputs appear to be filtered experimental results because the proposed model is built as an averaged model and the switching effect from the DC-DC converter is excluded. In the results for without battery case, the output voltages and power have more fluctuations compared to the case of with battery operation due to the effect from the load converter without a load smoothing operation by the battery. As a result, the DC bus voltage is less stable compared to the battery operation case, giving more RMS errors compared to with battery case. Without battery operation, there is no load sharing so the DC voltage set-point should be constant around 540V except for the fluctuations due to the DC bus voltage measurement. In Fig. 11(b),

since the proposed simulation model does not include the switching effect and cannot emulate the embedded controller dynamics perfectly, there are greater differences in the genset and battery power output than the Simscape model as seen in Fig. 11(b4 and b5). Therefore, these differences make the major differences in the voltage set-point and the measured DC bus voltage between the simulations and the experiment as seen in Fig. 11(b2 and b3). For example, the first major difference in 70s is due to the voltage set-point mismatch with the manufacturer's PMS, and the second major difference is due to the power mismatch in the DC-DC converter between 160s and 230s due to the different control tuning parameters. Nevertheless, the RMS errors are still within the acceptable range when it is compared to the errors produced by the Simscape model. This shows the validity of the proposed model.

The experimental measurements in the DC bus voltage and its set-point show the same trends with the simulation results in Fig. 11(b) confirming the validity of the model for the load sharing scheme. At 30s, since the power increasing rate of the battery is faster than the genset, the voltage set-point is slightly decreased and it is rising until 100s due to the constant power increase of the genset. Then, the genset is relatively keeping its load until 150s so the voltage set-point has no much difference. Then, the battery power rapidly decreases at 160s for charging operation with increasing the DC bus voltage set-point (rapidly in simulation but constantly in the experiment), and the DC bus voltage set-point becomes stable until 200s as the battery output power becomes stable. In this way, the results show that the validity of the proposed control method for load sharing can be also effective in the real system.

V. Conclusion

In this paper, comprehensive dynamic modeling and stability analysis of onboard DC hybrid power systems has been presented as a generic framework to be used for the control system design in different control levels such as local controllers and load-sharing/PMS level. The proposed model has been used to analyze the system stability in the small-signal domain and time-domain and to identify the dynamic modes related to the interaction of multi-layer control system with the power system. Here, the tested controllers use the PI regulator as an efficient and practical controller. For better tuning of the controllers, the interactive electro-mechanical modes of the DC SPS are taken into the system analysis and the results show that these modes shape the system dynamics. Based on the stability analysis, controllers are suggested in PMS-level and low-level to ensure the system stability under unequal load sharing between the power units, such as gensets and ESS. In the modified PMS, the voltage references are generated and are given to the AFE rectifiers considering their power set-point, resulting in an improved load sharing control.

To emulate the real ship operation, the system model is tested with the real ship data and various ESS functions. The results show that the ESS can contribute to the stabilization of the SPS, besides its main function to improve fuel efficiency. In each case, the analytical stability has been verified with the time-domain simulation. Finally, the simulation results are validated with the laboratory experiments under unequal load sharing between the power units. The experimental tests are repeated and compared with the replicated model in various operating modes such as with and without battery. The results show the effectiveness and fidelity of the proposed model.

References

[1] M. R. Miyazaki, A. J. Sørensen, N. Lefebvre, K. K. Yum, and E. Pedersen, "Hybrid Modeling of Strategic Loading of a Marine Hybrid Power Plant With Experimental Validation," *IEEE Access*, vol. 4, http://dx.doi.org/10.1109/ACCESS.2016.2629000DOI 10.1109/ACCESS.2016.2629000, pp. 8793–8804, 2016.

[2] P. Ghimire, D. Park, M. K. Zadeh, J. Thorstensen, and E. Pedersen, "Shipboard Electric Power Conversion: System Architecture, Applications, Control, and Challenges [Technology Leaders]," *IEEE Electrification Mag.*, vol. 7, http://dx.doi.org/10.1109/MELE.2019.2943948DOI 10.1109/MELE.2019.2943948, no. 4, pp. 6–20, Dec. 2019.

[3] Z. Jin, G. Sulligoi, R. Cuzner, L. Meng, J. C. Vasquez, and J. M. Guerrero, "Next-Generation Shipboard DC Power System: Introduction Smart Grid and dc Microgrid Technologies into Maritime Electrical Netowrks," *IEEE Electrification Mag.*, vol. 4, http://dx.doi.org/10.1109/MELE.2016.2544203DOI 10.1109/MELE.2016.2544203, no. 2, pp. 45–57, Jun. 2016.

[4] H. Alafnan, M. Zhang, W. Yuan, J. Zhu, J. Li, M. Elshiekh, and X. Li, "Stability Improvement of DC Power Systems in an All-Electric Ship Using Hybrid SMES/Battery," *IEEE Trans. Appl. Supercond.*, vol. 28, http://dx.doi.org/10.1109/TASC.2018.2794472DOI 10.1109/TASC.2018.2794472, no. 3, pp. 1–6, Apr. 2018.

[5] M. K. Zadeh, L. Saublet, R. Gavagsaz-Ghoachani, B. Nahid-Mobarakeh, S. Pierfederici, and M. Molinas, "Energy management and stabilization of a hybrid DC microgrid for transportation applications," in *2016 IEEE Applied Power Electronics Conference and Exposition (APEC)*, http://dx.doi.org/10.1109/APEC.2016.7468355DOI 10.1109/APEC.2016.7468355, pp. 3397–3402, Mar. 2016.

[6] Y. Son, S. Lee, S. Ko, Y. Kim, and S. Sul, "Maritime DC Power System With Generation Topology Consisting of Combination of Permanent Magnet Generator and Diode Rectifier," *IEEE Trans. Transp. Electrification*, vol. 6, http://dx.doi.org/10.1109/TTE.2020.2992474DOI 10.1109/TTE.2020.2992474, no. 2, pp. 869–880, Jun. 2020.

[7] U. Javaid, F. D. Freijedo, D. Dujic, and W. van der Merwe, "Dynamic Assessment of Source-Load Interactions in Marine MVDC Distribution," *IEEE Trans. Ind. Electron.*, vol. 64, http://dx.doi.org/10.1109/TIE.2017.2674597DOI 10.1109/TIE.2017.2674597, no. 6, pp. 4372–4381, Jun. 2017. [Online]. Available: http://ieeexplore.ieee.org/document/7862776/

[8] *Governing Fundamentals and Power Management*. Woodward Reference Manual 26260, Fort Collins, CO, 2004.

[9] A. D. Paquette, M. J. Reno, R. G. Harley, and D. M. Divan, "Sharing Transient Loads : Causes of Unequal Transient Load Sharing in Islanded Microgrid Operation," *IEEE Ind. Appl. Mag.*, vol. 20, http://dx.doi.org/10.1109/MIAS.2013.2288408DOI 10.1109/MIAS.2013.2288408, no. 2, pp. 23–34, Mar. 2014.

[10] F. D. Kanellos, G. J. Tsekouras, and N. D. Hatziargyriou, "Optimal Demand-Side Management and Power Generation Scheduling in an All-Electric Ship," *IEEE Trans. Sustain. Energy*, vol. 5, http://dx.doi.org/10.1109/TSTE.2014.2336973DOI 10.1109/TSTE.2014.2336973, no. 4, pp. 1166–1175, Oct. 2014.

[11] Y. Zhang, X. Qu, M. Tang, R. Yao, and W. Chen, "Design of Nonlinear Droop Control in DC Microgrid for Desired Voltage Regulation and Current Sharing Accuracy," *IEEE J. Emerg. Sel. Top. Circuits Syst.*, vol. 11, http://dx.doi.org/10.1109/JETCAS.2021.3049810DOI 10.1109/JETCAS.2021.3049810, no. 1, pp. 168–175, Mar. 2021.

[12] Z.-X. Xiao, H.-M. Li, H.-W. Fang, Y.-Z. Guan, T. Liu, L. Hou, and J. M. Guerrero, "Operation Control for Improving Energy Efficiency of Shipboard Microgrid Including Bow Thrusters and Hybrid Energy Storages," *IEEE Trans. Transp. Electrification*, vol. 6, http://dx.doi.org/10.1109/TTE.2020.2992735DOI 10.1109/TTE.2020.2992735, no. 2, pp. 856–868, Jun. 2020.

[13] Z. Jin, L. Meng, J. M. Guerrero, and R. Han, "Hierarchical Control Design for a Shipboard Power System With DC Distribution and Energy Storage Aboard Future More-Electric Ships," *IEEE Trans. Ind. Inform.*, vol. 14, http://dx.doi.org/10.1109/TII.2017.2772343DOI 10.1109/TII.2017.2772343, no. 2, pp. 703–714, Feb. 2018.

[14] X. Zhaoxia, Z. Tianli, L. Huaimin, J. M. Guerrero, C. Su, and J. C. Vásquez, "Coordinated Control of a Hybrid-Electric-Ferry Shipboard Microgrid," *IEEE Trans. Transp. Electrification*, vol. 5, http://dx.doi.org/10.1109/TTE.2019.2928247DOI 10.1109/TTE.2019.2928247, no. 3, pp. 828–839, Sep. 2019.

[15] A. Riccobono, M. Cupelli, A. Monti, E. Santi, T. Roinila, H. Abdollahi, S. Arrua, and R. A. Dougal, "Stability of Shipboard DC Power Distribution: Online Impedance-Based Systems Methods," *IEEE Electrific. Mag.*, vol. 5, http://dx.doi.org/10.1109/MELE.2017.2718858DOI 10.1109/MELE.2017.2718858, no. 3, pp. 55–67, Sep. 2017. [Online]. Available: http://ieeexplore.ieee.org/document/8025651/

[16] U. Javaid, F. D. Freijedo, W. van der Merwe, and D. Dujic, "Stability Analysis of Multi-Port MVDC Distribution Networks for All-Electric Ships," *IEEE J. Emerg. Sel. Top. Power Electron.*, http://dx.doi.org/10.1109/JESTPE.2019.2926380DOI 10.1109/JESTPE.2019.2926380, pp. 1–1, 2019.

[17] G. Sulligoi, D. Bosich, G. Giadrossi, L. Zhu, M. Cupelli, and A. Monti, "Multiconverter Medium Voltage DC Power Systems on Ships: Constant-Power Loads Instability Solution Using Linearization via State Feedback Control," *IEEE Trans. Smart Grid*, vol. 5, http://dx.doi.org/10.1109/TSG.2014.2305904DOI 10.1109/TSG.2014.2305904, no. 5, pp. 2543–2552, Sep. 2014. [Online]. Available: http://ieeexplore.ieee.org/document/6813657/

[18] G. Sulligoi, A. Vicenzutti, V. Arcidiacono, and Y. Khersonsky, "Voltage Stability in Large Marine-Integrated Electrical and Electronic Power Systems," *IEEE Trans. Ind. Appl.*, vol. 52, http://dx.doi.org/10.1109/TIA.2016.2544833DOI 10.1109/TIA.2016.2544833, no. 4, pp. 3584–3594, Jul. 2016.

[19] D. Park and M. K. Zadeh, "Dynamic Modeling and Stability Analysis of Onboard DC Power System for Hybrid Electric Ships," in *2019 IEEE Transportation Electrification Conference and Expo (ITEC)*, http://dx.doi.org/10.1109/ITEC.2019.8790505DOI 10.1109/ITEC.2019.8790505, pp. 1–6, Jun. 2019.

[20] M. Raza, E. Prieto-Araujo, and O. Gomis-Bellmunt, "Small-Signal Stability Analysis of Offshore AC Network Having Multiple VSC-HVDC Systems," *IEEE Trans. Power Deliv.*, vol. 33, http://dx.doi.org/10.1109/TPWRD.2017.2725982DOI 10.1109/TPWRD.2017.2725982, no. 2, pp. 830–839, Apr. 2018.

[21] L. He, Y. Li, Z. Shuai, J. M. Guerrero, Y. Cao, M. Wen, W. Wang, and J. Shi, "A Flexible Power Control Strategy for Hybrid AC/DC Zones of Shipboard Power System With Distributed Energy Storages," *IEEE Trans. Ind. Inform.*, vol. 14, http://dx.doi.org/10.1109/TII.2018.2849201DOI 10.1109/TII.2018.2849201, no. 12, pp. 5496–5508, Dec. 2018.

[22] D. Park and M. Zadeh, "Modeling and Predictive Control of Shipboard Hybrid DC Power Systems," *IEEE Trans. Transp. Electrification*, http://dx.doi.org/10.1109/TTE.2020.3027184DOI 10.1109/TTE.2020.3027184, pp. 1–1, 2020.

[23] W. Xie, M. Han, W. Cao, J. M. Guerrero, and J. C. Vasquez, "System-Level Large-Signal Stability Analysis of Droop-Controlled DC Microgrids," *IEEE Trans. Power Electron.*, vol. 36, http://dx.doi.org/10.1109/TPEL.2020.3019311DOI 10.1109/TPEL.2020.3019311, no. 4, pp. 4224–4236, Apr. 2021.

[24] N. Bottrell, M. Prodanovic, and T. C. Green, "Dynamic Stability of a Microgrid With an Active Load," *IEEE Trans. Power Electron.*, vol. 28, http://dx.doi.org/10.1109/TPEL.2013.2241455DOI 10.1109/TPEL.2013.2241455, no. 11, pp. 5107–5119, Nov. 2013.

[25] M. K. Zadeh, R. Gavagsaz-Ghoachani, B. Nahid-Mobarakeh, S. Pierfederici, and M. Molinas, "Stability analysis of hybrid AC/DC power systems for more electric aircraft," in *2016 IEEE Applied Power Electronics Conference and Exposition (APEC)*, http://dx.doi.org/10.1109/APEC.2016.7467910DOI 10.1109/APEC.2016.7467910, pp. 446–452, Mar. 2016.

[26] J. Chen and J. Chen, "Stability Analysis and Parameters Optimization of Islanded Microgrid With Both Ideal and Dynamic Constant Power Loads," *IEEE Trans. Ind. Electron.*, vol. 65, http://dx.doi.org/10.1109/TIE.2017.2756588DOI 10.1109/TIE.2017.2756588, no. 4, pp. 3263–3274, Apr. 2018.

[27] M. K. Zadeh, R. Gavagsaz-Ghoachani, S. Pierfederici, and B. Nahid-

[28] F. Göthner, R. E. Torres-Olguin, J. Roldán-Pérez, A. Rygg, and O.-M. Midtgård, "Apparent Impedance-Based Adaptive Controller for Improved Stability of a Droop-Controlled Microgrid," *IEEE Trans. Power* Mobarakeh, "Stability Analysis and Dynamic Performance Evaluation of a Power Electronics-Based DC Distribution System With Active Stabilizer," *IEEE J. Emerg. Sel. Top. POWER Electron.*, vol. 4, no. 1, p. 10, 2016.

Electron., vol. 36, http://dx.doi.org/10.1109/TPEL.2021.3050615DOI 10.1109/TPEL.2021.3050615, no. 8, pp. 9465–9476, Aug. 2021.

[29] M. K. Zadeh, R. Gavagsaz-Ghoachani, J.-P. Martin, S. Pierfederici, B. Nahid-Mobarakeh, and M. Molinas, "Discrete-Time Tool for Stability Analysis of DC Power Electronics-Based Cascaded Systems," *IEEE Trans. Power Electron.*, vol. 32, http://dx.doi.org/10.1109/TPEL.2016.2526740DOI 10.1109/TPEL.2016.2526740, no. 1, pp. 652–667, Jan. 2017. [Online]. Available: http://ieeexplore.ieee.org/document/7401083/

[30] J. F. Hansen, A. K. Ådnanes, and T. I. Fossen, "Mathematical Modelling of Diesel-Electric Propulsion Systems for Marine Vessels," *Mathematical and Computer Modelling of Dynamical Systems*, vol. 7, http://dx.doi.org/10.1076/mcmd.7.3.323.3641DOI 10.1076/mcmd.7.3.323.3641, no. 3, pp. 323–355, Sep. 2001. [Online]. Available: http://www.tandfonline.com/doi/abs/10.1076/mcmd.7.3.323.3641

[31] J. Machowski, Z. Lubosny, J. W. Bialek, and J. R. Bumby, *Power System Dynamics: Stability and Control*. John Wiley & Sons, 2008, Jun. 2020.

[32] P. W. Sauer and M. A. Pai, *Power System Dynamics and Stability*. Upper Saddle River, NJ, USA: Prentice-Hall, 1998.

[33] K. Areerak, S. V. Bozhko, G. M. Asher, and D. W. P. Thomas, "DQ-transformation approach for modelling and stability analysis of AC-DC power system with controlled PWM rectifier and constant power loads," in *2008 13th International Power Electronics and Motion Control Conference*, http://dx.doi.org/10.1109/EPEPEMC.2008.4635567DOI 10.1109/EPEPEMC.2008.4635567, pp. 2049–2054, Sep. 2008.

[34] M. Chen and G. A. Rincon-Mora, "Accurate electrical battery model capable of predicting runtime and I-V performance," *IEEE Trans. Energy Convers.*, vol. 21, http://dx.doi.org/10.1109/TEC.2006.874229DOI 10.1109/TEC.2006.874229, no. 2, pp. 504–511, Jun. 2006.

[35] E. Skjong, T. A. Johansen, M. Molinas, and A. J. Sørensen, "Approaches to Economic Energy Management in Diesel–Electric Marine Vessels," *IEEE Trans. Transp. Electrification*, vol. 3, http://dx.doi.org/10.1109/TTE.2017.2648178DOI 10.1109/TTE.2017.2648178, no. 1, pp. 22–35, Mar. 2017.

[36] M. B. Othman, N. P. Reddy, P. Ghimire, M. K. Zadeh, A. Anvari-Moghaddam, and J. M. Guerrero, "A Hybrid Power System Laboratory: Testing Electric and Hybrid Propulsion," *IEEE Electrification Mag.*, vol. 7, http://dx.doi.org/10.1109/MELE.2019.2943982DOI 10.1109/MELE.2019.2943982, no. 4, pp. 89–97, Dec. 2019.

Daeseong Park was born in Seoul, Republic of Korea, in 1987. He received the B.Sc.degree in naval architecture and ocean engineering with Cum Laude from Seoul National University, Republic of Korea, in 2013, and the M.Sc. degree in Marine Technology from the Norwegian University of Science and Technology (NTNU), Trondheim, Norway, in 2018. He is currently working toward the Ph.D. degree in the Department of Marine Technology at NTNU. He worked as an assistant engineer for ship systems in Daewoo Shipbuilding and Marine Engineering (DSME) from 2013 to 2016. His current research interests include modeling, control and stability analysis of shipboard power systems.

Mehdi Zadeh received the Ph.D. degree in Electrical Engineering from NTNU, Trondheim, Norway, in 2016. From 2016 to 2017, he was with the power electronics industry, working on the development of battery charging systems. In 2017, he joined the Marine Technology Centre at NTNU in Trondheim, where he is currently an Associate Professor of Hybrid Power Systems and the director of the Marine Electrification Research Lab. His main research interests include onboard power electronics, marine electrification, low-emission and autonomous shipping, and offshore renewable energy systems.